The effects of molecular weight, evaporation rate and polymer concentration on pillar formation in drying poly(ethylene oxide) droplets

K.A. Baldwin[a,b], D.J. Fairhurst[a,*]

[a]*School of Science and Technology, Nottingham Trent University, Clifton Lane, Nottingham, NG11 8NS, United Kingdom*
[b]*School of Physics and Astronomy, University of Nottingham, Nottingham NG7 2RD, United Kingdom*

Abstract

Typically, when droplets of dilute suspensions are left to evaporate the final dry deposit is the familiar coffee-ring stain, with nearly all the solute deposited at the initial contact line. Contrastingly, in previous work we have shown that sessile droplets of poly(ethylene oxide) (PEO) solutions form tall central pillars (or monoliths) during a 4-stage drying process. We show that a dimensionless Péclet-type number Pe, a ratio of the competing advective and diffusive motion of the dissolved polymer, which incorporates the effects of evaporation rate, initial concentration c_0 and the polymer diffusion coefficient, to determine whether the droplet will form a pillar or a flat deposit. In this work we vary concentration up to $c_0 = 0.5$ and molecular weight M_w between 3.35kg/mol and 600kg/mol and find that in ambient conditions with $c_0 = 0.1$ pillars only form for a limited range, $35 \leq M_w \leq 200$ kg/mol. This observation is in contrast to the the Péclet argument in which high molecular weight polymers with a slow self-diffusion should still form pillars. We present various experimental measurements attempting to resolve this discrepancy: crossover time-scale for viscoelastic behaviour; fast diffusion of an entangled network; and droplet viscosity or contact line friction.

Keywords: droplet, evaporation, polymer, deposit, poly(ethylene oxide),

---

*Corresponding author
Email addresses: `kyle.baldwin@ntu.ac.uk` (K.A. Baldwin), `david.fairhurst@ntu.ac.uk` (D.J. Fairhurst)

1. Introduction

The seminal work of Deegan et.al. in 1997 [1] proposed a simple explanation for the common occurrence of coffee-ring stains: enhanced evaporation at the pinned contact line induces outward flow to replenish solvent loss and sweeps suspended material to the contact line where it is deposited as a ring stain. In the subsequent years understanding the competing dynamic processes within evaporating sessile droplets has become an increasingly complex and interesting subject, encompassing many experimental factors such as: the solvent evaporation rate [2, 3]; interactions between solvent, solute, vapour and substrate [4, 5]; phase transitions within the droplet [6, 7]; internal convection currents [8, 9, 10]; solute diffusion [11, 12, 13]; and the shape of suspended particles [14]. As well as to understand the fundamental science, motivation comes from a variety of industrial applications such as ink-jet printing [15], drying paints and varnishes, evaporative cooling [16], and effective chemical delivery in crop spraying.

One of the goals of ongoing research into drying sessile droplets is to remove the coffee-ring stain, a phenomenon typically considered an obstacle when attempting to create uniform deposits. Phenomena which have been observed to achieve this goal include: capillary forces [17]; surface-mediated repulsion of irregular shaped particles [14]; Marangoni flow induced by surface tension gradients [10]; and electrowetting [18].

In previous work [19] we studied the drying behaviour of sessile droplets of aqueous poly(ethylene oxide) (PEO) solution, at a fixed molecular weight $M_\mathrm{w} = 100\mathrm{kg/mol}$, and observed the coffee-ring effect only at low mass fractions ($c_0 \leq 0.03$). However, at higher concentrations the outward flow driving the dissolved polymer to the contact line counter-intuitively leads to the majority of the dissolved polymer being deposited in a tall central pillar. To explain this the drying process was broken down into 4 stages: classical pinned drying during which the contact line is stationary; precipitation-induced receding contact line[1]; boot-strap building as the liquid droplet is lifted by

---

[1]The exact mechanism behind the receding stage is currently unknown but candidates include an increase of the contact angle between liquid and solid (autophobic effect [20]), squeezing of the liquid by the crystallising front, or viscoelastic recoil of the concentrated

the crystallising solid; and finally a slow contraction as the remaining water evaporates.

In a 1 dimensional model [21, 22] pillar formation was shown to be controlled by a Péclet type ratio of the evaporation rate, $-\dot{V}$ (where V is droplet volume), which drives the polymer to the contact line during pinned drying, and the gradient diffusion coefficient of the polymer, D_G, which in the absence of evaporation would homogenize the solution, along with initial droplet parameters of mass concentration c_0, droplet base radius R, contact angle θ. In this work, as supported by various theoretical modelling approaches to particle dynamics during sessile droplet drying [1, 10, 23], we assume that the majority of evaporation over the surface of a droplet occurs in a narrow wedge very close to the contact line. If it is also assumed that evaporation across the surface of this wedge is constant, then by geometrically resolving the flux across this wedge from droplet to atmosphere we find that in a spherical cap droplet the Péclet number follows:

$$Pe \approx \frac{\dot{V}}{D_G R \sin\theta} \frac{c_0}{c_{\text{sat}} - c_0} \tag{1}$$

where the saturation concentration $c_{\text{sat}} = 0.60 \pm 0.062$. Although the model is only based on initial values and does not consider the 3 dimensional geometry of the droplet, it showed reliable universality in predicting whether a droplet with given initial parameters would form a pillar.

PEO is a widely used linear polymer and unique amongst its homologues for its high solubility in water [24]. Its behaviour in water is well studied, and although some uncertainties persist regarding the nature of molecular clustering [25] many of its properties are well known [26]: for example, when modelled as an ideal chain it has an effective freely-jointed chain step-length (length of a Kuhn monomer) of $b = 1.1$nm and molecular weight per Kuhn monomer of $M_0 = 137$g/mol. In dilute solutions it is well characterised by the statistics of the self-avoiding chain so the radius of gyration R_G scales with the number of Kuhn steps $N = M_{\text{w}}/N_0$ as $R_G \sim N^{3/5}$. Also, the gradient diffusion coefficient is equal to the self-diffusion coefficient D_0 and scales as $D_{\text{G}} = D_0 \sim R_G^{-1} \sim M_{\text{w}}^{-3/5}$, showing that for longer molecules D_0 is lower. On increasing concentration, the transition from dilute to semi-dilute polymer solutions occurs when the spheres of radius R_{G} around each

_____

polymer solution.

3

polymer molecule are closely packed, at a concentration termed the overlap concentration c^*. The interactions between molecules can not be ignored, and the chain configurations are no longer described by the self-avoiding walk of a dilute solution. The value c^* decreases with increasing molecular weight $c^* \sim M_\mathrm{w}/R_g^3 \sim M_\mathrm{w}^{-4/5}$. This means that high molecular weight molecules overlap at very low concentrations. For semi-dilute solutions above c^*, the value of the gradient diffusion coefficient is modified by a concentration dependent term $D_\mathrm{G} \sim D_0(c^*/c)^{1/2} \sim M_\mathrm{w}^{-1}$ [27] so decreases even more rapidly with increasing M_w than in dilute solutions. Consequently, the predictions from the Pèclet argument would suggest that for both dilute and semi-dilute solutions at a fixed concentration, higher molecular weight PEO will preferentially form pillars as diffusion will not be sufficient to homogenise the solution. Below, we present an experimental investigation of this prediction by systematically varying mass concentration between 1 and 50% (respectively, the lower and upper limits are given by the concentrations at which pillar formation could not be induced and solutions could not be mixed), molecular weight between 3.35 and 600kg/mol, and drying rates by a factor of 20 (limited by the lower pressure at which droplets freeze).

2. Material and methods

Solutions were prepared mixing distilled deionised water with PEO from two suppliers spanning a range of M_w values between 3.35 and 600kg/mol and initial mass fractions c_0 between 0.02 and 0.5. Solutions were left to equilibrate for at least 24 hours, and placed onto a roller mixer before use to eliminate any possible sedimentation effects. Table 1 lists details of each sample and supplier with M_w values and uncertainties quoted from manufacturers figures. Values of D_0, R_G and c^* are calculated from [26] using $R_G = bN^{3/5}$ and $c^* = 3Nb^3/4\rho\pi R_g^3$ where $\rho = 1064\mathrm{kg/m}^3$ is the density of PEO.

For each measurement, a droplet with initial volume $V_0 = 10\mu\mathrm{L}$ was slowly pipetted onto a clean glass microscope coverslip. The coverslip was then placed into either a sealed perspex chamber (with dimensions $15 \times 10 \times 11\mathrm{cm}$) to reduce atmospheric disturbances, or a cylindrical low pressure chamber (diameter 8.6cm, height 5.4cm), connected to a Cole Parmer diaphragm pump and a pressure sensor, for precise manual control of the pressure down to 15mbar. At ambient lab conditions relative humidity in the chamber was stable at $50\pm5\%$ and was increased by introducing satu-

| M_w | Supplier | Product | R_G | D_0 | c^* |
kg/mol		code	nm	$\mu m^2/s$	
3.35±0.3	Sigma	P4338	2.94	116.7	0.325
8±1	Sigma	P4463	4.91	69.9	0.167
20±4	Sigma	95172	8.41	40.8	0.083
~ 35	Sigma	P4646	11.69	29.4	0.054
~ 100	Sigma	181986	21.67	15.8	0.0242
100 ±50	Polysci.	06104	21.67	15.8	0.0242
200±100	Polysci.	17503	32.58	10.5	0.014
~ 300	Sigma	182001	41.35	8.3	0.0105
300 ±150	Polysci.	06105	41.35	8.3	0.0105
600±300	Polysci.	06106	62.16	5.5	0.0062

Table 1: Details of the various PEO samples used. The physical properties (radius of gyration R_G, self-diffusion coefficient D_0 and overlap concentration c^*) are calculated using PEO properties given in the text. An estimation of the uncertainty in the molecular weight value is included if provided by the supplier.

rated salt solutions (sodium chloride and potassium sulphate giving 75±2% and 81±2% respectively), and measured independently using an Omegaette HH311 probe, interfaced to the computer using the supplied software. Temperature in lab conditions remained constant at 22±1°C.

The droplet was illuminated by a diffuse light source, placed behind the droplet outside the chamber and a digital camera recorded images of the drying process every second. Droplets drying at atmospheric pressure were prepared and recorded as described by Baldwin et al. [21]. The rate of change of volume $\dot{V}$ was determined both by gravimetric means to an accuracy of ±1mg and by extracting the two dimensional droplet profile ($h(r)$) from the digital side-on images using ImageJ software (US National Institutes of Health). We use the position of the maximum droplet height $h_{max} = h(r_0)$ to define r_0 and the edge of the droplet is defined where $h(r = \pm R) = 0$, where R is the droplet base radius. Volume of rotation V was calculated numerically in Matlab using r_0 as the vertical axis of rotation.

3. Results and discussions

Figure 1 shows time lapse images of droplets with initial concentration $c_0 = 0.1$ during drying at ambient conditions, $T = 22 \pm 1°C$, $R_H = 50 \pm 5\%$ and PEO molecular weight $M_\mathrm{w} = 8$, 100 and 300kg/mol. The 4 stages of

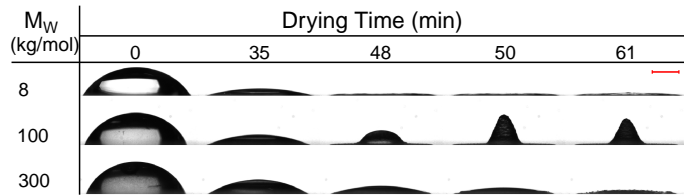| M_W (kg/mol)	Drying Time (min)				
	0	35	48	50	61
8					
100					
300					

Figure 1: Time lapse profile images of PEO solution droplets with initial concentration $c_0 = 0.1$ during drying at ambient conditions, recorded at 0, 35, 48, 50 and 61 minutes. PEO M_w=8, 100 and 300kg/mol in top middle and bottom rows respectively. Scale bar (red) represents 1mm.

drying (pinned drying, receding contact line, boot-strap building and slow contraction) can only be seen with $M_w = 100$kg/mol, suggesting that at ambient conditions for $c_0 = 0.1$ an intermediate range in chain length is required for pillar formation.

Also worth noting is that the initial contact angle θ_0 appears to increase with increasing M_w. This is due to slow spreading of these high viscosity droplets after deposition - spreading stopped in all droplets at approximately the same equilibrium contact angle. The cloudiness of higher molecular weight solutions is due to non-dissolving micron-sized aggregates of PEO formed during mixing, the origin of which is still under contention [25]. In previous experiments [21] these aggregates were removed by passing the solution through a 0.45μm filter, and through careful density and viscosity measurements of the solutions after filtration, they have been shown to account for a very small percentage ($< 5\%$) of the total PEO in solution. Furthermore these aggregates seem to have little effect on the final morphology, and so were not removed here.

Figure 2 shows the final profiles of varying concentration and molecular weight. While the saturation concentration remains roughly constant at $c_{sat} \approx 0.6$ irrespective of M_w, solutions with a very high viscosity were either too slow to mix or too difficult to pipette into spherical cap droplets of the desired volume, and so these were omitted.

Figure 3 shows the effects of atmospheric pressure and molecular weight on the final profiles of the deposit dried from droplets with initial concentration $c_0 = 0.1$. For each value of M_w it is clear that lowering the pressure, and thus increasing the evaporation rate, encourages pillar formation, as at $P = 20$mbar, all samples except the $M_w = 3.35$kg/mol form pillars, some of which are so tall and unstable they fall over during their growth. This
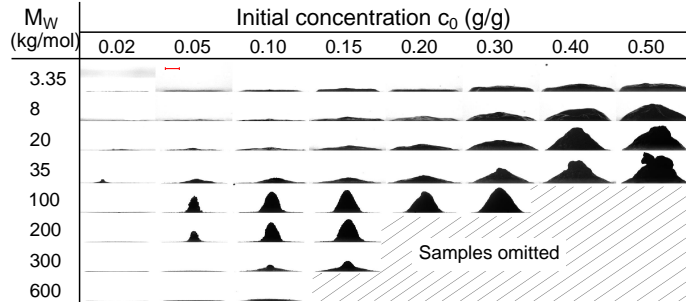
Figure 2: Profile images of fully dried PEO solution droplets varying initial concentration c_0 and M_w at ambient conditions. Shaded region in lower right indicates solutions that were either too slow to mix or too viscous to pipette accurately. The (red) scale bar represents 1mm.

aspect of the results is in agreement with the Péclet model, which argues that increasing the relative effect of evaporation rate against polymer diffusion causes earlier polymer build up at the contact line, leading to taller fully dried pillar structures. While we have not increased atmospheric pressure in this study, we would predict that, much as with the high humidity results published previously [21], a significantly reduced evaporation rate would lead to a Péclet number less than unity and flat uniform deposits. Interestingly, Fig. 3 also confirms that pillar formation only occurs in the narrow range $20 \leq M_w \leq 200$kg/mol at ambient conditions with $c_0 = 0.1$, although this range does broaden with reduced pressure and increasing concentration.

So, although the Péclet argument captures some of the pillar-formation behaviour, the dependence on molecular weight is not as expected: samples with high M_w do not easily form pillars. Consequently, additional explanations are required, and we explore three possibilities below with further experimental data.

Firstly, it is known from frequency-dependent rheological studies of high molecular weight entangled polymer solutions that there is a characteristic time-scale τ, which separates viscous- from elastic-type behaviour. At low frequency shear oscillation the polymeric material will have time to rearrange and flow whereas at faster frequencies, the polymer network is elastically deformed and returns to its original configuration when the stress is removed. Following this line of argument would suggest that at sufficiently high evaporation rates, when the droplet would need to respond rapidly to the shape changes imposed by volume loss, the polymer within the droplet
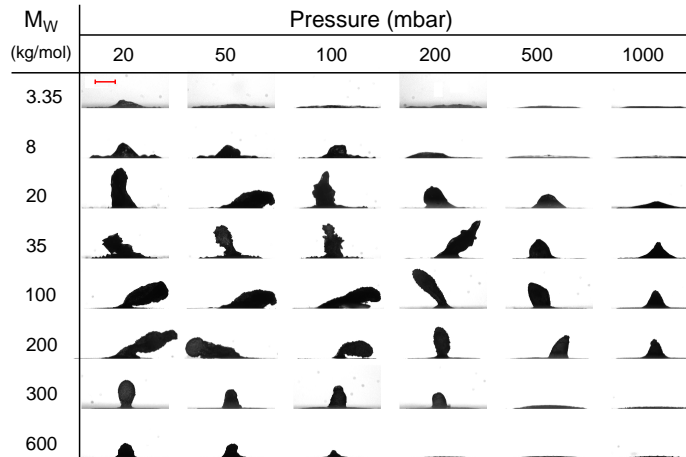
7

M_W	Pressure (mbar)					
(kg/mol)	20	50	100	200	500	1000
3.35						
8						
20						
35						
100						
200						
300						
600						

Figure 3: Profile images of fully dried PEO solution droplets, varying M_w and atmospheric pressure. Initial concentration $c_0 = 0.1$. The red scale bar represents 1mm.

would deform elastically and there would be no accumulation of molecules at the contact line. For slower evaporation, polymer molecules would flow and preferential deposition at the contact line would occur, leading to pillar formation. Using cone and plate geometry on a TA Instruments CSL^{2}100 rheometer we performed oscillation rheology experiments and found the characteristic time for samples with $M_\mathrm{w} = 300$kg/mol to vary between $\tau = 0.03$s for $c_0 = 0.05$ up to $\tau = 0.9s$ for $c_0 = 0.2$. However, the results at low pressure show that pillars form *more* readily at fast evaporation rates, whereas the visco-elastic prediction suggests the opposite: that solutions will behave more like solids and not form pillars. For this reason, we discard this explanation.

An alternative hypothesis considers the variation of the diffusion constant with both concentration and molecular weight. For dilute and semi-dilute solutions, polymer chains diffuse as individual entities, controlled by self diffusion, and low molecular weight molecules will still diffuse quickly, preventing pillar formation. However, above the entanglement concentration c_e, the inter-connected network reacts to concentration gradients much more quickly than individual molecules do: in fact the diffusion coefficient is inversely proportional to the entanglement length, the distance between adjacent entanglement points, so will increase at higher concentrations. Fast network diffusion of high molecular weight polymer would lead to less significant concentration gradients, less precipitation at the edge and may explain the lack of pillars seen in these solutions. To test this hypothesis, we prepared seven
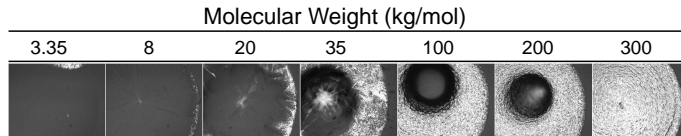
8

Figure 4: Polarising-light microscopy images showing spherulite formation in droplets of varying molecular weight. All images were taken after one hour under similar drying conditions.

samples with initial concentration $c_0 = 0.1$ and low initial contact angle. The droplets were observed while they evaporated using a polarising microscope. In Fig.4 we show images taken after one hour. Precipitation occurs earlier for the samples with higher molecular weight, with the $M_w = 300\text{kg/mol}$ sample showing first spherulites at the edge after only 22 minutes. Given our observation that c_{sat} does not change significantly with M_w over the range considered here, early appearance of spherulites indicates higher concentration and slower diffusion. Consequently, these experiments do not support the network diffusion hypothesis.

A third hypothesis is that the crystallisation front which drives the receding contact line is insufficiently strong to push back droplets with high M_w. This could be due either to increased droplet viscosity or to additional effects of adhesion combined in the contact line friction [28]. Careful studying of the images suggests that this may indeed be the case, as a skin of solid polymer can sometimes be seen to build up on the free surface of high M_w droplets, which eventually covers the droplet preventing pillar formation. This suggest that other criteria are important in determining pillar formation in addition to the Péclet argument discussed earlier. Further experiments to measure the viscosity of very high concentration droplets (which are difficult to prepare) and to estimate the forces generated at the contact line by the solid deposit will be needed to quantify this hypothesis.

An order or magnitude prediction can be obtained from scaling arguments, which show that the viscosity of entangled polymer solutions in good solvents varies as $\eta \sim (c/c^*)^{3.75} \sim c^{3.75} M_w^3$ [26]. On Fig.5 we have plotted all droplets with $c_0 = 0.1$, indicating by the symbol whether each forms a pillar or a puddle. The horizontal axis is M_w and the vertical axis is the product PeD_G which is calculated from purely experimental values using Equation 1: we use the values of V measured from the image sequence to calculate $\dot{V}$; R, θ and $c_0 = 0.1$ are known from the initial droplet properties; and we take
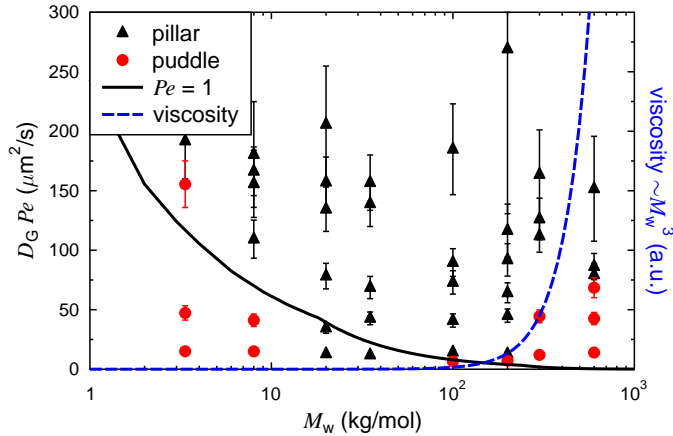
Figure 5: Plot of all $c_0 = 0.1$ droplets, with (black) triangles indicating those that formed pillars and (red) circles those that formed puddles. The horizontal axis is polymer molecular weight and vertical axis the product PeD_G which increases with evaporation rate. Error bars reflect uncertainties in measuring the evaporative flux accurately. The solid line corresponds to $Pe = 1$ and the dashed (blue) line represents $\eta \sim M_w^3$ indicating how viscosity depends on molecular weight.

$c_{\mathrm{sat}} = 0.6$. The theoretical boundary between pillar and puddle at $Pe = 1$ is plotted as a solid black line given by the value of D_G calculated as described above for both dilute and semi-dilute regimes. Finally, a line proportional to M_w^3, representing the effect of viscosity is also plotted, scaled arbitrarily. We can see that the pillar-forming region is bounded on the low molecular weight side by the $Pe = 1$ line and on the high molecular weight side by the viscosity curve, providing encouragement that these two effects are critical in controlling pillar formation.

4. Conclusions

We have shown that a high Péclet number is a necessary but not sufficient criteria for the formation of tall central monoliths in evaporating droplets of PEO solution. Values of $Pe > 1$ lead to preferential crystallisation at the contact line. However this does not always lead to pillar formation: in some cases, with high molecular weight polymers, the viscosity of the droplet or contact line friction is sufficient to resist the force pushing the droplet inwards, so the solid forms as a skin over the droplet instead. Further experiments are required to fully validate this model, in particular with regards

10

the viscosity measurements. However, the insight that pillar formation is determined by a combination of evaporation rate, diffusion and viscosity will guide future work and help in the identification of other candidate systems which may form central pillars on drying.

5. Acknowledgements

[1] R. Deegan, O. Bakajin, T. Dupont, G. Huber, S. Nagel, T. Witten, Nature 389 (1997) 827–829.

[2] A.-M. Cazabat, G. Geoffroy, Soft Matter 6 (2010) 2591–2612.

[3] A. G. Marín, H. Gelderblom, D. Lohse, J. H. Snoeijer, Physical Review Letters 107 (2011).

[4] S. Rowan, M. Newton, F. Driewer, G. McHale, Journal of Physical Chemistry B 104 (2000) 8217–8220.

[5] G. Li, K. Graf, Phys Chem Chem Phys 11 (2009) 7137–44.

[6] L. Pauchard, C. Allain, Europhysics Letters 62 (2003) 897–903.

[7] F. Parisse, C. Allain, Langmuir 13 (1997) 3598–3602.

[8] M. Kaneda, K. Hyakuta, Y. Takao, H. Ishizuka, J. Fukai, Langmuir 24 (2008) 9102–9109.

[9] K. H. Kang, S. J. Lee, C. M. Lee, K. I.S., Measurement Science and Technology 15 (2004) 1104–1112.

[10] H. Hu, R. G. Larson, Journal of Physical Chemistry B 106 (2002) 1334–1344.

[11] W. Brown, Polymer 26 (1985) 1647–1650.

[12] U. Zettl, S. T. Hoffmann, F. Koberling, G. Krausch, J. Enderlein, L. Harnau, M. Ballauff, Macromolecules 42 (2009) 9537–9547.

[13] K. Ozawa, T. Okuzono, M. Doi, Japanese journal of applied physics 45 (2006) 8817–8822.

[14] P. J. Yunker, T. Still, M. A. Lohr, A. Yodh, Nature 476 (2011) 308–311.

[15] B. J. de Gans, P. C. Duineveld, U. S. Schubert, Advanced Materials 16 (2004) 203–213.

[16] K. Sefiane, R. Bennacer, Journal of Fluid Mechanics 667 (2011) 260–271.

[17] B. M. Weon, J. H. Je, Physical Review E 82 (2010) 015305.

[18] H. B. Eral, D. M. Augustine, M. H. G. Duits, F. Mugele, Soft Matter 7 (2011) 4954–4958.

[19] D. Willmer, K. A. Baldwin, C. Kwartnik, D. J. Fairhurst, Physical Chemistry Chemical Physics 12 (2010) 3998–4004.

[20] G. Reiter, R. Khanna, Langmuir 16 (2000) 6351–6357.

[21] K. A. Baldwin, M. Granjard, D. I. Willmer, K. Sefiane, D. J. Fairhurst, Soft Matter 7 (2011) 7819–7826.

[22] K. A. Baldwin, S. Roest, D. J. Fairhurst, K. Sefiane, M. E. R. Shanahan, Journal of Fluid Mechanics 695 (2012) 321–329.

[23] K. L. Maki, S. Kumar, Langmuir (2011).

[24] B. Hammouda, Journal of Polymer Science Part B - Polymer Physics 44 (2006) 3195–3199.

[25] B. Hammouda, D. Ho, S. Kline, Macromolecules 37 (2004) 6932–6937.

[26] M. Rubinstein, R. H. Colby, Polymer physics, volume 105, Oxford University Press New York, 2003.

[27] M. Doi, S. F. Edwards, The Theory of Polymer Dynamics, Clarendon, 1998.

[28] M. J. de Ruijter, T. D. Blake, J. De Coninck, Langmuir 15 (1999) 7836–7847.